Available online at www.sciencedirect.com
ScienceDirect
Journal of the European Ceramic Society 30 (2010) 413–418
www.elsevier.com/locate/jeurceramsoc

The synthesis and microwave dielectric properties of $Mg_3B_2O_6$ and $Mg_2B_2O_5$ ceramics

Urban Došler*, Marjeta Maček Kržmanc, Danilo Suvorov

"Jožef Stefan" Institute, Jamova 39, 1000 Ljubljana, Slovenia

Available online 24 June 2009

Abstract

Single-phase $Mg_3B_2O_6$ and $Mg_2B_2O_5$ ceramics were synthesized and then structurally and dielectrically characterized. The highest *Qxf* value of 230,900 GHz was obtained for a $Mg_3B_2O_6$ ceramic with a density of 97% and 1000-μm grains. Considerably lower *Qxf* values (10,000–32,000 GHz) were determined for the $Mg_2B_2O_5$ ceramic. $Mg_3B_2O_6$ and $Mg_2B_2O_5$ exhibited permittivities (ε) of 7.2 and 6.2–7.0, respectively. Both ceramics showed negative temperature coefficients of resonant frequency (τ_f) of −18 to −45 ppm/°C.

Keywords: Calcination; Dielectric properties; Grain growth; Grain size; Substrate

1. Introduction

The number of investigations of the synthesis and crystallization of various glass–ceramic materials has increased recently because of their potential for use in versatile chemical, thermal, biological and dielectric applications.[1] Glass–ceramics also have a good potential for use in low-temperature co-fired ceramic (LTCC) technology as substrates, with calcium borosilicate ($CaO–B_2O_3–SiO_2$) glass–ceramics being some of the most important LTCC substrate materials used in microelectronics packaging. They have been widely investigated by many researchers because of their excellent dielectric properties.[2–9]

In contrast to the $CaO–B_2O_3–SiO_2$ system, the crystallization of $MgO–B_2O_3–SiO_2$ glass–ceramics and their dielectric behaviour have not yet been reported. Our preliminary research indicates that this latter glass–ceramics system could be easy to synthesize and exhibits promising dielectric and sintering properties. Knowledge about the structural and dielectric characteristics of the individual crystalline phases, which crystallized from the $MgO–B_2O_3–SiO_2$ glass, will help us to understand the properties of this glass–ceramic system. In the $MgO–B_2O_3–SiO_2$ ternary system there are three binary systems: $MgO–SiO_2$, $SiO_2–B_2O_3$ and $MgO–B_2O_3$. The dielectric properties of the compounds from the last of these binary systems ($Mg_3B_2O_6$, $Mg_2B_2O_5$, MgB_4O_7) have not been well investigated.

Magnesium borates ($Mg_3B_2O_6$, $Mg_2B_2O_5$, MgB_4O_7) have received much attention due to their versatile, potential applications, such as anti-wear and anti-corrosion materials, thermoluminescent phosphors and as catalysts useful for the conversion of hydrocarbons.[10,11] The syntheses of nanorods, nanowires, nanobelts and nanotubes prevail among the published methods for preparing $Mg_2B_2O_5$ and $Mg_3B_2O_6$ materials.[10–14] However, there is some literature data about the solid-state synthesis of $Mg_2B_2O_5$ and $Mg_3B_2O_6$ from the pure initial oxides.[15]

In this study, the synthesis, sintering behaviour and microwave dielectric properties of crystalline $Mg_2B_2O_5$ and $Mg_3B_2O_6$ are systematically investigated and discussed. The main focus of this investigation was on a determination of the correlations between the microstructural characteristics and the microwave dielectric properties.

2. Experimental

The $Mg_3B_2O_6$- and $Mg_2B_2O_5$-based ceramics were synthesized from MgO and B_2O_3 using solid-state reaction techniques. Prior to weighing, the MgO and B_2O_3 powders were dried for 12 h at 500 °C and 100 °C, respectively. These dried powders were then homogenized in acetone and repeatedly pre-reacted with intermediate grinding and milling. The detailed pre-reaction conditions for the synthesis of $Mg_3B_2O_6$ and $Mg_2B_2O_5$ are presented in Table 1. The loss of B_2O_3,

* Corresponding author. Tel.: +386 1 477 3991; fax: +386 1 251 9385.
E-mail address: urban.dosler@ijs.si (U. Došler).

0955-2219/$ – see front matter © 2009 Elsevier Ltd. All rights reserved.
doi:10.1016/j.jeurceramsoc.2009.05.049

Table 1
Pre-reactions and sintering conditions of $Mg_3B_2O_6$ and $Mg_2B_2O_5$.

Material	Pre-reactions temperatures (°C)	Sintering temperature (°C)	Structure
$Mg_3B_2O_6$	600, 900, 1000, 1100, 1200	1200–1300	S.G. *Pnm*
$Mg_2B_2O_5$	600, 900, 1000, 1100, 1200	1250–1280	S.G. $P\bar{1}$

The pre-reaction time at each temperature was 10 h.

which occurred during the pre-reactions, was compensated by weighing an 11 wt.% and 14 wt.% excess of B_2O_3 for the $Mg_3B_2O_6$ and $Mg_2B_2O_5$, respectively.

Prior to sintering, the powders were milled in acetone with Y-stabilized ZrO_2 balls ($d = 3$ mm) for 2 h to a median particle size of 1 μm. The milled powders were then uniaxially pressed under a pressure of 100 MPa to obtain green compacts with a diameter of 12 mm and a thickness of around 4 mm. The green pellets were sintered at different temperatures for various periods of time and then cooled to room temperature. The cooling rate from the sintering temperature (T_s) was either fast or slow, with the latter being a controlled cooling rate of 2 °C/min. Fast cooling refers to uncontrolled cooling in the furnace as a result of natural convection, conduction and radiation from the sintering temperature to room temperature. The rate of fast cooling was estimated to be 10 °C/min.

The progress of the reaction after each pre-reaction step was monitored by powder X-ray diffraction (XRD) using a D4 Endeavor (Bruker AXS, Karlsruhe, Germany) X-ray diffractometer with Cu Kα radiation (1.5406 Å). The X-ray powder diffraction data were collected from $10° < 2\theta < 70°$ with a step of 0.02°, a counting time of 3 s, using divergence and antiscattering slits with a length of 20 mm (denoted as V20). The D4 Endeavor X-ray diffractometer was equipped with a scintillation counter and a Ni filter.

The sintering of the $Mg_3B_2O_6$ and $Mg_2B_2O_5$ pellets was observed with a heating microscope (EM 201, Hesse Instruments, Osterode, Germany), which monitored the change of the pellets' silhouettes during the heating up with a defined heating profile. The heating rate in both experiments was 10 °C/min. Thermogravimetric (TG) and differential scanning calorimetry (DSC) analyses were performed on a Jupiter 449 simultaneous thermal analysis (STA) instrument coupled with a mass spectrometer (MS) (403C Aëoloss, Netzsch, Selb, Germany).

The thermal etching of the polished samples was performed at 50° below the sintering temperature.

The densities of the sintered specimens were measured using Archimedes' method with acetone. The literature data of 3.086 g/cm^3 (PDF 38-1475) and 2.91 g/cm^3 (PDF 15-0537) were used for the theoretical densities of the $Mg_3B_2O_6$ and the $Mg_2B_2O_5$.[16] The relative densities (ρ_r) were obtained by comparing the measured densities with the theoretical ones.

The microstructural studies of the samples were conducted with a scanning electron microscope (SEM) JXA 840A, JEOL, Tokyo, coupled with an energy-dispersive X-ray spectrometer (EDX) and software (Series II X-ray microanalyzer, Tracor Northern, Middleton, WI).

The radio-frequency (RF) dielectric measurements were performed at 1 MHz on Au-plated disk capacitors using a high-precision LCR meter (Agilent 4284 A). The permittivity measured at 1 MHz was used to determine the appropriate $TE_{01\delta}$ mode in the microwave (MW) frequency range. The MW dielectric properties were characterized using the dielectric resonator method, described by Krupka et al.[17], using a network analyzer (HP 8719C). The permittivity and dielectric losses ($\tan\delta$) were calculated at the resonant conditions. The Q values were calculated from the $\tan\delta$ values in accordance with the equation $Q = 1/\tan\delta$. To determine the temperature coefficient of resonant frequency (τ_f) the test cavities were inserted into a temperature-controlled chamber. The dielectric characteristics of the samples were analyzed in the temperature range from 20 °C to 60 °C.

3. Results and discussion

3.1. Synthesis of $Mg_3B_2O_6$ and $Mg_2B_2O_5$

The synthesis of $Mg_3B_2O_6$ and $Mg_2B_2O_5$ from stoichiometric ratios of the initial oxides did not lead to single-phase ceramics. The presence of MgO in the $Mg_3B_2O_6$ ceramics as well as the presence of $Mg_3B_2O_6$ in the $Mg_2B_2O_5$ ceramics could be an indication of the evaporation of B_2O_3 during the pre-reactions and sintering (Figs. 1 and 2, curve d). The loss of B_2O_3 was compensated for by the addition of excess B_2O_3 at the beginning of the synthesis. The required amounts of excess B_2O_3 were determined experimentally by the preparation of initial mixtures with a 5–15% excess of B_2O_3. These initial mixtures were pre-reacted under the conditions described in Table 1. The required amount of excess B_2O_3 for $Mg_3B_2O_6$ and $Mg_2B_2O_5$ was selected on the basis of the single-phase composition of the powders annealed at 1200 °C. In the XRD pattern of $Mg_3B_2O_6$ with 10 wt.% excess of B_2O_3 a small amount of secondary MgO phase was present after annealing at 1200 °C, whereas

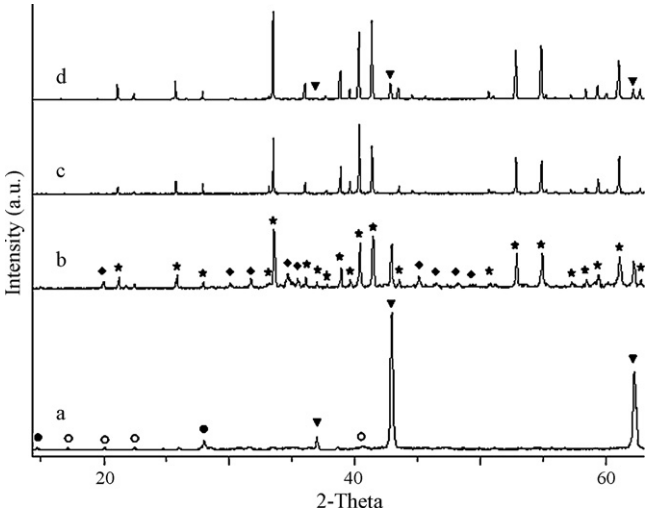

Fig. 1. X-ray powder diffraction pattern of the $Mg_3B_2O_6$ (nominal composition (1300 °C), curve d) and $Mg_3B_2O_6$ with an 11 wt.% excess of B_2O_3 after pre-reaction at 600 °C (a), 900 °C (b) and 1300° (c). Denotation of the crystalline phases: (⋆) $Mg_3B_2O_6$, (⧫) $Mg_2B_2O_5$, (▼) MgO, (●) H_3BO_3, and (◯) MgB_4O_7.

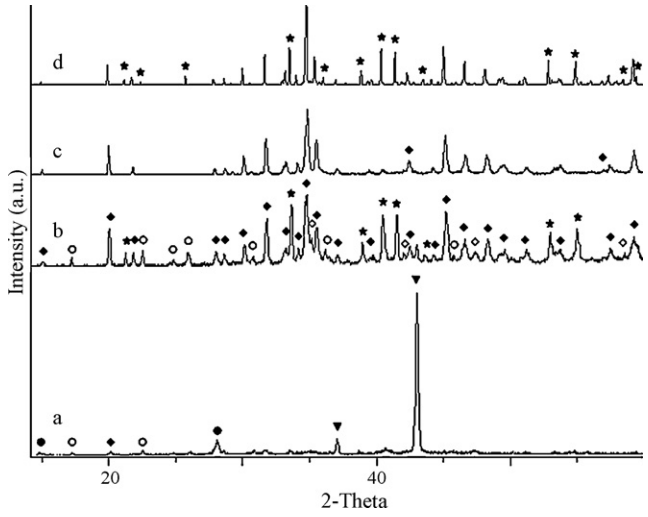

Fig. 2. X-ray powder diffraction pattern of the $Mg_2B_2O_5$ (nominal composition (1250 °C), curve d) and $Mg_2B_2O_5$ with a 14 wt.% excess of B_2O_3 after pre-reaction at 600 °C (a), 900 °C (b) and 1250 °C (c). Denotation of the crystalline phases: (⋆) $Mg_3B_2O_6$, (♦) $Mg_2B_2O_5$ (triclinic), (◊) $Mg_2B_2O_5$ (monoclinic), (▼) MgO, (●) H_3BO_3, and (◯) MgB_4O_7.

the $Mg_2B_2O_5$ phase appeared in the case of 13 wt.% excess of B_2O_3. The $Mg_3B_2O_6$ with 11 wt.% of excess B_2O_3 annealed at 1200 °C, as well as at 1300 °C, was single phase on the basis of the results from the X-ray diffractometry (Fig. 1, curve c). For the $Mg_2B_2O_5$, 14 wt.% of excess B_2O_3 was selected, since this amount led to single-phase $Mg_2B_2O_5$ at 1200 °C and at 1250 °C (Fig. 2, curve c).

The temperature for the first pre-reaction at 600 °C was chosen on the basis of the exothermic peak at 600–800 °C in the DSC curve, which was attributed to the crystallization of the magnesium borates. In addition to the crystallization peaks above 600 °C, the DSC curve of the homogenized, initial powders also revealed two strong endothermic peaks below 200 °C (Fig. 3). The mass spectrometry of the evolved gas revealed that the mass loss in the TG curve and these endothermic peaks coincided with

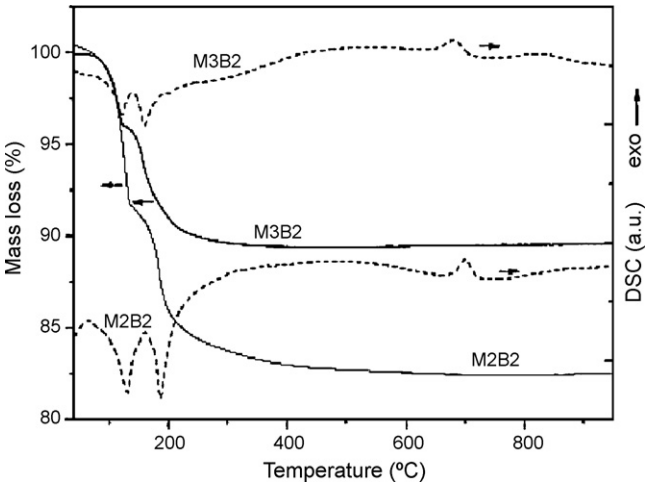

Fig. 3. TG (—) and DSC (- - - -) curves of homogenized $Mg_3B_2O_6$ (denoted as M3B2) and $Mg_2B_2O_5$ (denoted as M2B2) powders with 11 wt.% and 14 wt.% of B_2O_3, respectively.

the removal of water. Taking into account the literature data, these processes below 200 °C could be attributed to the decomposition of H_3BO_3.[18] Although the B_2O_3 was dried before weighing, the B_2O_3 bound water during the homogenization in air, forming H_3BO_3. The diffraction lines of crystalline H_3BO_3 can also be seen in the XRD pattern of the pre-reacted powders at 600 °C (Figs. 1 and 2, curves a). Due to the low intensity of the H_3BO_3 diffraction lines, the majority of the B_2O_3 remained in the form of an amorphous oxide.

During the pre-reaction of the homogenized powder with a stoichiometry of $Mg_3B_2O_6$ (11 wt.% excess of B_2O_3) at 600 °C the MgB_4O_7 and $Mg_2B_2O_5$ phases started to form. A significant amount of unreacted MgO and traces of H_3BO_3 were also present in the pre-reacted powder at this temperature. At 900 °C $Mg_3B_2O_6$ appeared as the dominant phase (Fig. 1, curve b). The secondary phases identified at this temperature were MgO and $Mg_2B_2O_5$; however, both of them completely disappeared at 1000 °C.

From the similar crystallization peak at 600–800 °C (Fig. 3) it appears that the pre-reaction of $Mg_2B_2O_5$ (with 14 wt.% excess of B_2O_3) also started at 600 °C. However, despite the crystallization of MgB_4O_7 and $Mg_2B_2O_5$, the majority of the MgO and B_2O_3 remained unreacted at this temperature (Fig. 2, curve a). In the XRD pattern of the $Mg_2B_2O_5$ powder pre-reacted at 900 °C the diffraction lines of all the magnesium borates (MgB_4O_7, $Mg_2B_2O_5$, $Mg_3B_2O_6$) and MgO were present (Fig. 2, curve b). With the subsequent pre-reaction at 1000 °C, the $Mg_2B_2O_5$ phase increased, while the MgB_4O_7, $Mg_3B_2O_6$ and MgO phases disappeared. The monoclinic (S.G. $P2_1/a$) and triclinic (S.G. $P\bar{1}$) crystal modifications of the $Mg_2B_2O_5$ were present up to 1000 °C. Only the triclinic modification was found in the samples annealed at $T \geq 1100$ °C.

3.2. Sintering and microstructural characteristics

With regard to the sintering behaviour observed by means of the heating microscope, the densification of the $Mg_3B_2O_6$ started above 1000 °C (Fig. 4). In order to prepare ceramics with high density, $Mg_3B_2O_6$ was sintered at 1200 °C and 1300 °C. When the microstructures of the $Mg_3B_2O_6$ ceramics sintered under various conditions were compared considerable differences in the grain size and the porosity were observed. The ceramics sintered at 1300 °C (20 h) and cooled slowly consisted of ~1000-μm grains, containing some closed porosity (Fig. 5a and b). In the $Mg_3B_2O_6$ ceramics sintered for a shorter time (10 h) at 1300 °C and cooled rapidly the grain sizes are in a broad range from 10 μm to 1000 μm. In addition to the large elongated grains there are also areas with smaller grains of a few tens of μm (Fig. 5c and d). Only small grains of 10–50 μm were present in the ceramics sintered at 1200 °C (Fig. 5e). These ceramics showed porous microstructures and the closed porosity was replaced by open porosity. Intensive grain growth and closed porosity, as it is present in the $Mg_3B_2O_6$ ceramics sintered at 1300 °C (Fig. 5a–c), usually occur as a consequence of liquid-phase formation. With regard to the phase diagram reported by Mutluer et al. the admixture of MgO or $Mg_2B_2O_5$ to $Mg_3B_2O_6$ decreases the melting temperature, and the reported

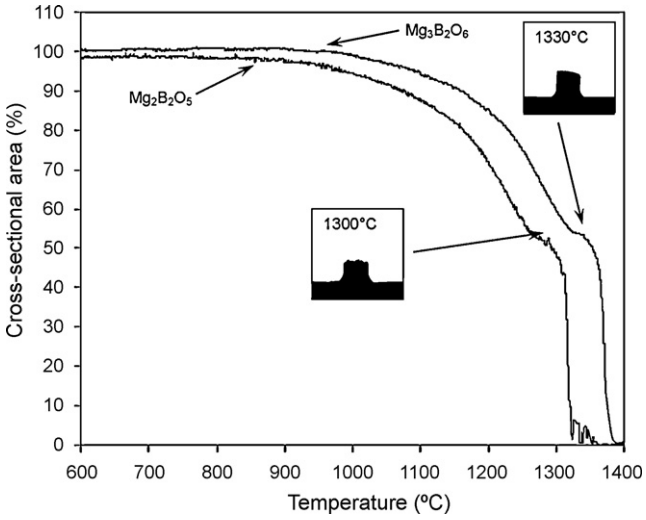

Fig. 4. Sintering profiles of the milled $Mg_3B_2O_6$ and $Mg_2B_2O_5$ powders observed with a heating microscope.

eutectic temperature between $Mg_3B_2O_6$ and MgO is 1333 °C. On the basis of this we assume that the admixture of MgO could not cause the formation of a liquid phase during sintering at 1300 °C. The reported temperature of the incongruent melting of $Mg_2B_2O_5$ at 1312 °C is much closer to our sintering temperature at 1300 °C. Since we did not detect any $Mg_2B_2O_5$ by XRD we assume that its concentration is below 2%. Another reason for the liquid-phase formation could also be the low-melting-point glassy phase, which is often present in systems based on

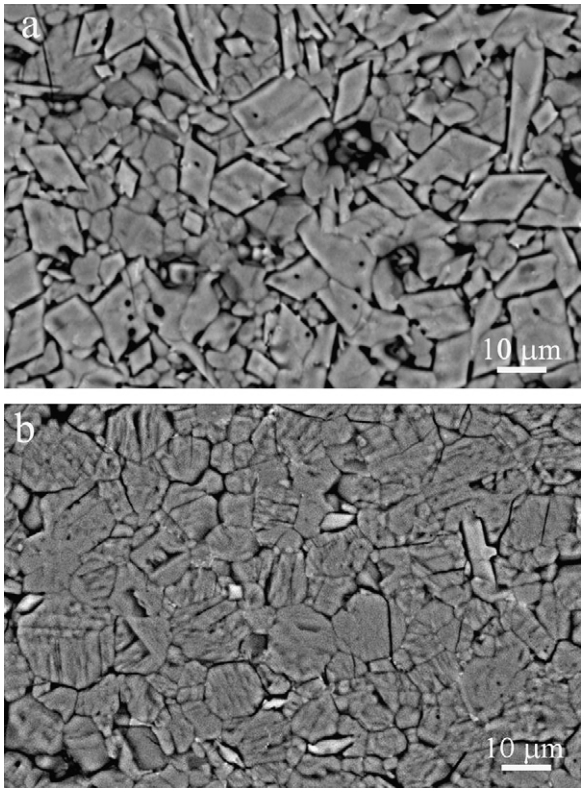

Fig. 6. Scanning electron micrographs of the thermally etched $Mg_2B_2O_5$ ceramics sintered at 1280 °C for 10 h, cooled fast (a) and sintered at 1280 for 20 h cooled with a slow cooling rate of 2 °C/min (b).

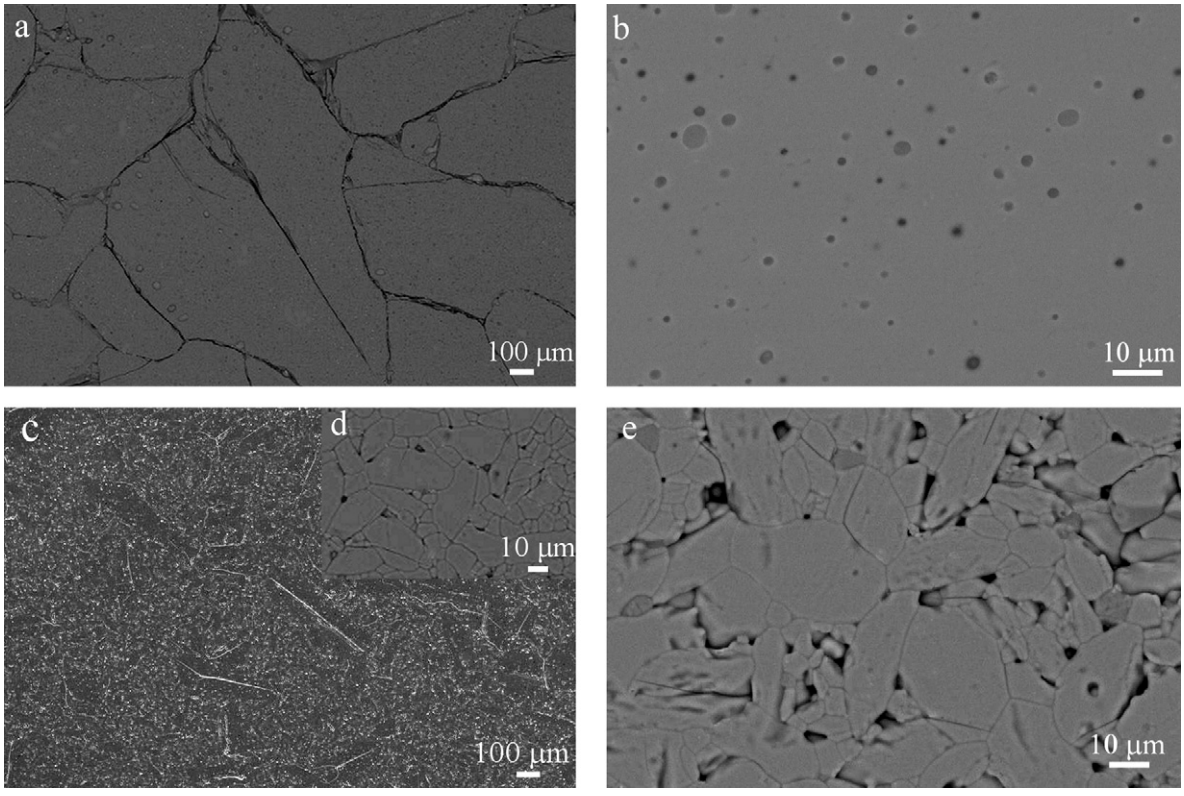

Fig. 5. Scanning electron micrographs of the thermally etched $Mg_3B_2O_6$ ceramics sintered at 1300 °C for 20 h and cooled with a cooling rate of 2 °C/min (a and b), sintered at 1300 °C for 10 h and cooled fast (c and d) and sintered at 1200 °C for 10 h and cooled fast (e).

Table 2
Microwave dielectric properties of $Mg_3B_2O_6$ and $Mg_2B_2O_5$ ceramics.

Material			$Mg_3B_2O_6$	
Ts (°C)	1200 °C/10 h	1300 °C/10 h	1300 °C/10 h	1300 °C/20 h
Cooling	Fast	Fast	2 °C/min	2 °C/min
ε	6.8	7.4	7.0	7.2
Qxf (GHz)	57,900	150,000	230,900	220,300
f_o (GHz)	12.1	11.9	11.8	11.6
τ_f (ppm/°C)	−37	−36	−42	−45
ρ_r (%)	91	97	95	96
Material			$Mg_2B_2O_5$	
Ts (°C)	1250 °C/10 h	1250 °C/20 h	1280 °C/10 h	1280 °C/20 h
Cooling	Fast	Fast	Fast	2 °C/min
ε	7.0	6.6	6.6	6.2
Qxf (GHz)	18,400	19,100	19,800	32,100
f_o (GHz)	12.0	11.9	12.3	12.6
τ_f (ppm/°C)	−41	−46	−41	−18
ρ_r (%)	95	97	94	95

B_2O_3. Although the reasons for grain growth are not entirely understood, the majority of investigations indicate that the temperature and the duration of the annealing have a bigger larger influence on the grain growth than the cooling rate.

The densification of the $Mg_2B_2O_5$ also started above 1000 °C (Fig. 4). However, in the sintered $Mg_2B_2O_5$ ceramics (Ts = 1250–1280 °C) no such exaggerated grain growth, like in the case of $Mg_3B_2O_6$, was observed. An SEM micrograph of a thermally etched sample revealed grains with a size of ~10 μm. Some of the grains in the fast-cooled sample (Fig. 6a) are euhedral, while in the slow-cooled sample they are more anhedral (Fig. 6b). Further investigations are needed to provide an explanation for this difference.

3.3. Microwave dielectric characterization

It is generally known that an extrinsic phenomenon such as porosity causes a detrimental deviation from the intrinsic dielectric properties of the materials. A low level of porosity (<5%) decreases the permittivity but does not have a major influence on the microwave dielectric losses. In addition, a porosity of more than 5% also has a detrimental effect on the dielectric losses. In contrast to the permittivity and the dielectric losses the τ_f is reported to be less sensitive to the porosity.[19] Density measurements on the sintered $Mg_3B_2O_6$ and $Mg_2B_2O_5$ revealed that it was very difficult to prepare ceramics with relative densities higher than 97%. The microwave dielectric properties, together with the density data, are presented in Table 2. In accordance with the higher density, the permittivity (ε = 7.2) of the $Mg_3B_2O_6$ ceramics sintered at 1300 °C was higher than the permittivity (ε = 6.8) of the ceramics sintered at 1200 °C (Table 2). The permittivity of the $Mg_2B_2O_5$ varied from 6.2 to 7.0.

The $Mg_3B_2O_6$ ceramics sintered at 1300 °C showed considerably higher Qxf values than the ceramics sintered at 1200 °C (Table 2). Besides the different densities, these two types of ceramics also exhibited a large difference in the grain size. The highest Qxf values over 220,000 GHz (at 11.8 GHz) were observed for the ceramics that were sintered at 1300 °C for 10 or 20 h and cooled slowly from the sintering temperature with a controlled cooling rate of 2 °C/min. These ceramics consisted of large grains (~1000 μm) with some closed porosity. According to the density measurements the porosity was about 4–5%. Porosities in this range were reported to have no significant influence on the dielectric losses.[19] The ceramics sintered at 1300 °C (10 h) and cooled rapidly contained areas of large (500–1000 μm) and small grains (10–50 μm) (Fig. 5c and d). The Qxf value of this ceramic was 150,000 GHz. In the ceramics sintered at 1200 °C the grains were only a few tens of μm in size (Fig. 5e) and the Qxf value was 57,900 GHz. $Mg_3B_2O_6$ was already reported to exhibit a high Qxf value of 150,000 GHz,[20] but the properties of the ceramics prepared in this study exceeded this value. The ceramics that exhibited a Qxf > 200,000 GHz consisted of 500–1000-μm grains, whereas the Qxf values fell below 150,000 GHz in the case of a few 10-μm grains. It is known that grain boundaries increase the dielectric losses, and that there is a smaller concentration of grain boundaries in the ceramics with large grains. Nevertheless, further investigations are needed to find out whether the variation in the grain size is the only reason for this large difference in the Qxf values.

In contrast to the $Mg_3B_2O_6$ ceramics, the $Mg_2B_2O_5$ exhibited much lower Qxf values in the range from 18,400 GHz to 32,100 GHz. Due to a relative density of ≤95% there is a significant extrinsic contribution to the measured Qxf values. The τ_f values of $Mg_3B_2O_6$ and $Mg_2B_2O_5$ were in the range −18 to −45 ppm/°C (Table 2).

4. Conclusions

Single-phase $Mg_3B_2O_6$ and $Mg_2B_2O_5$ ceramics were prepared with the solid-state reaction technique using an excess of 11 wt.% and 14 wt.% B_2O_3, respectively. The synthesis of the $Mg_3B_2O_6$ and $Mg_2B_2O_5$ was performed in several subsequent pre-reaction steps. In both cases the synthesis of the target $Mg_3B_2O_6$ or $Mg_2B_2O_5$ was accompanied by the formation of other magnesium borates at a lower temperature (600 °C). At 900 °C $Mg_3B_2O_6$ appeared as the dominant phase; a higher

temperature (1000 °C) was required for the $Mg_2B_2O_5$ to become the prevailing phase. The sintering of both magnesium borates was performed at various temperatures from 1200 °C to 1300 °C. The permittivity of the $Mg_3B_2O_6$ ceramics was 6.8–7.4 and τ_f was in the range from −36 to −45 ppm/°C. The properties of the $Mg_3B_2O_6$-based ceramics from this study exceed the already reported *Qxf* values for this type of ceramic. Our investigations showed some indication of a correlation between the grain size and the *Qxf* value. The highest *Qxf* values of over 220,000 GHz were observed for the $Mg_3B_2O_6$ ceramics with ∼1000-μm grains. The $Mg_3B_2O_6$ ceramics that contained 10–50-μm grains exhibited a *Qxf* value below 150,000 GHz.

The permittivity (ε = 6.2–7.0) and τ_f (−18 to −41 ppm/°C) of the $Mg_2B_2O_5$ did not differ significantly from that of the $Mg_3B_2O_6$, while the *Qxf* values were considerably lower (*Qxf* = 18,400–32,100 GHz). The microstructural investigations of the sintered $Mg_2B_2O_5$ ceramics revealed the presence of 10-μm grains.

References

1. Tulyaganov, D. U., Agathopoulos, S., Ventura, J. M., Karakassides, M. A., Fabrichnaya, O. and Ferreira, J. M. F., Synthesis of glass–ceramics in the $CaO–B_2O_3–SiO_2$ system with B_2O_3, P_2O_5, Na_2O and CaF_2 additives. *J. Eur. Ceram. Soc.*, 2006, **26**, 1463–1471.
2. Zhu, H., Liu, M., Zhou, H., Li, L. and Lv, A., Study on properties of $CaO–B_2O_3–SiO_2$ system glass–ceramic. *Mater. Res. Bull.*, 2007, **42**, 1137–1144.
3. Chiang, C. C., Wang, S. F., Wang, Y. R. and Wei, W. C. J., Densification and microwave dielectric properties of $CaO–B_2O_3–SiO_2$ system glass–ceramics. *Ceram. Int.*, 2008, **34**, 599–604.
4. Jean, J. H., Chang, C. R. and Lei, C. D., Sintering of a crystallizable $CaO–B_2O_3–SiO_2$ glass with silver. *J. Am. Ceram. Soc.*, 2004, **87**, 1244–1249.
5. Chiang, C. C., Wang, S. F., Wang, Y. R. and Hsu, Y. F., Characterization of $CaO–B_2O_3–SiO_2$ glass–ceramics: thermal and electrical properties. *J. Alloys Compd.*, 2008, **461**, 612–616.
6. Lei, C. D. and Jean, J. H., Effect of crystallization on the stress required for constrained sintering of $CaO–B_2O_3–SiO_2$ glass–ceramics. *J. Am. Ceram. Soc.*, 2005, **88**, 599–603.
7. Chang, C. R. and Jean, J. H., Crystallization kinetics and mechanism of low dielectric, low-temperature, cofirable $CaO–B_2O_3–SiO_2$ glass–ceramics. *J. Am. Ceram. Soc.*, 1999, **82**, 1725–1732.
8. Wang, S. H. and Zhou, H. P., Densification and dielectric properties of $CaO–B_2O_3–SiO_2$ system glass ceramics. *Mater. Sci. Eng. B*, 2003, **99**, 597–600.
9. Hartmann, H. S., Crystallizable, low dielectric constant, low dielectric loss composition. US Patent 5,024,975, June 18, 1991.
10. Zeng, Y., Yang, H., Fu, W., Qiao, L., Chang, L., Chen, J. *et al.*, Synthesis of magnesium borate ($Mg_2B_2O_5$) nanowires, growth mechanism and their lubricating properties. *Mater. Res. Bull.*, 2008, **43**, 2239–2247.
11. Elssfah, E. M., Elsanousi, H. A., Zhang, J., Song, H. S. and Tang, C., Synthesis of magnesium borate nanorods. *Mater. Lett.*, 2007, **61**, 4358–4361.
12. Zhang, J., Li, Z. and Zhang, B., Formation and structure of single crystalline magnesium borate ($Mg_3B_2O_6$) nanobelts. *Mater. Chem. Phys.*, 2006, **98**, 195–197.
13. Li, Y., Fan, Z., Lu, J. G. and Chang, R. P. H., Synthesis of magnesium borate ($Mg_2B_2O_5$) nanowires by chemical vapor deposition method. *Chem. Mater.*, 2004, **16**, 2512–2514.
14. Qasrawi, A. F., Kayed, T. S., Mergen, A. and Gürü, M., Synthesis and characterization of $Mg_2B_2O_5$. *Mater. Res. Bull.*, 2005, **40**, 583–589.
15. Mutluer, T. and Timucin, M., Phase equilibria in the system $MgO–B_2O_3$. *J. Am. Ceram. Soc.*, 1975, **58**, 196–197.
16. PCPDFWIN Version 2.3, JCPDS-International Center for Diffraction Data, June 2001.
17. Krupka, J., Derzakowski, K., Riddle, B. and Jarvis, J. B., A dielectric resonator for measurements of complex permittivity of low loss dielectric materials as a function of temperature. *Meas. Sci. Technol.*, 1998, **9**, 1751–1756.
18. Sevim, F., Demir, F., Bilen, M. and Okur, H., Kinetic analysis of thermal decomposition of boric acid from thermogravimetric data. *Korean J. Chem. Eng.*, 2006, **23**(5), 736–740.
19. Valant, M. and Suvorov, D., Microstructural phenomena in low-firing ceramics. *Mater. Chem. Sci.*, 2003, **79**, 104–110.
20. Mori, N., Sugimoto, Y., Harada, J. and Higuchi, Y., Dielectric properties of new glass–ceramics for LTCC applied to microwave or millimeter-wave frequencies. *J. Eur. Ceram. Soc.*, 2006, **26**, 1925–1928.